Remote Sensing Precipitation: Sensors, Retrievals, Validations, and Applications

Yang Hong, Guoqiang Tang, Yingzhao Ma, Qi Huang, Zhongying Han, Ziyue Zeng, Yuan Yang, Cunguang Wang, and Xiaolin Guo

Contents

Abstract

Precipitation is one of the most important water cycle components. The chapter reviews modern instruments and techniques for global precipitation retrieval,

Y. Hong (✉)
State Key Laboratory of Hydroscience and Engineering, Department of Hydraulic Engineering, Tsinghua University, Beijing, China

School of Civil Engineering and Environmental Science, University of Oklahoma, Norman, OK, USA
e-mail: yanghong@ou.edu

G. Tang · Y. Ma · Q. Huang · Z. Han · Z. Zeng · Y. Yang · C. Wang · X. Guo
State Key Laboratory of Hydroscience and Engineering, Department of Hydraulic Engineering, Tsinghua University, Beijing, China

X. Li, H. Vereecken (eds.), *Observation and Measurement of Ecohydrological Processes*, Ecohydrology, https://doi.org/10.1007/978-3-662-48297-1_4

including weather radars and satellites. Some of the most popular global multi-satellite precipitation products are introduced, including PERSIANN-CCS, TMPA, and IMERG. In addition, we extend to the typical regional and global studies about the assessment of various products and their application in flood detection and prediction.

Keywords
Remote sensing · Precipitation · Sensors · Retrievals · Validations · Applications

Introduction

Precipitation plays a vital role in understanding the mechanism and interaction of global water and energy balance and is the main input of hydrometeorological models and climate studies (Hong et al. 2007; Kidd and Huffman 2011). Researchers can hardly conduct simulations of the water cycle and eco-hydrological process without accurate precipitation inputs. Traditionally, people can measure rainfall and snowfall using various types of ground-based rain gauges. However, rain gauge-based techniques for precipitation observations have nonnegligible limitations in eco-hydrology research due to large spatial nonuniformity and temporal availability in rainfall fields inherently. And unfortunately, the number of ground rain gauges continues to decline over the world (Stokstad 1999; Shiklomanov et al. 2002). In addition, rain gauges have trouble observing precipitation in the oceans, polar areas, and mountainous regions which attracts more and more attention in the context of climate change (Ma et al. 2016).

Fortunately, the development of remote sensing techniques promotes the capability of humans in observing global precipitation. Weather radars and space-based meteorological satellites are two major remote sensing techniques in precipitation observation. After World War II, weather radars have dramatically improved our ability to measure precipitation at high temporal and spatial resolutions (Farbry et al. 1994; Morin et al. 1995; Harris et al. 2001; Berne et al. 2004). For example, the United States has built a dense radar network, namely, Next-Generation Weather Radar (NEXRAD) consisting of around 160 high-resolution S-band Doppler weather radars (Heiss et al. 1990; Vivekanandan et al. 1990). Regional-scale studies can be performed across the United States, Western Europe, and a few other regions across the globe. In China, more than 100 S-band and C-band weather radars have also been installed and been applied in meteorological and hydrological research (Fang et al. 2002). However, weather radar systems are still inadequate for obtaining global precipitation and suffer from similar problems with gauges such as limited spatial coverage, particularly in oceanic, remote, or undeveloped regions.

Currently, the only practical way to achieve global precipitation observation is space-based meteorological satellites (Hong et al. 2012; Tang et al. 2016a). Satellite-based precipitation estimates have great advantages in terms of spatial coverage compared with rain gauges and weather radars. Moreover, satellite measurements are

continuous and uniform and can avoid the high cost of ground observation networks (Hong et al. 2016). Global satellite-based rainfall products are currently mainly based on passive microwave (PMW), calibrated infrared (IR), and PMW plus IR observations. IR sensors are on geostationary Earth orbit (GEO) satellites which provide precipitation estimates at high temporal resolutions, but the accuracy of IR-based rainfall estimates is generally not good due to the indirect linkage between IR signals and precipitation. PMW sensors are onboard low Earth orbiting (LEO) satellites and can provide precipitation estimation with a more direct link to rain and ice particles. Currently, some countries, such as the United States and China, have been trying to put PMW sensors onto GEO satellites which, if realized, can promote the capability of observing rainfall from space significantly. Active microwave sensors can provide the most accurate estimation of rainfall and snowfall, i.e., the Ku-band precipitation radar (PR) onboard the TRMM satellite (Simpson et al. 1988), the W-band Cloud Profiling Radar (CPR) onboard the CloudSat and the Ku-/Ka-band Dual-frequency Precipitation Radar (DPR) onboard the GPM Core Observatory (Hou et al. 2014). However, those spaceborne precipitation radars also suffer from long revisiting periods.

There have been great numbers of multi-satellite precipitation products since the launch of TRMM in late 1997, such as Multi-satellite Precipitation Analysis (TMPA) (Huffman et al. 2007), Climate Prediction Center (CPC) MORPHing technique (CMORPH) (Joyce et al. 2004), Precipitation Estimation from Remotely Sensed Information using Artificial Neural Networks (PERSIANN) (Sorooshian et al. 2000), PERSIANN Cloud Classification System (PERSIANN-CCS) (Hong et al. 2004), and Global Satellite Mapping of Precipitation (GSMaP) (Kubota et al. 2007). Those products are generally based on IR, MW, and rain gauge data which have promoted our knowledge of global precipitation and the development of hydrological and eco-hydrological models.

This chapter first provides an overview of remotely sensed rainfall, including satellite sensors and weather radars, precipitation retrieval algorithms, and global precipitation products. Then we briefly introduce the validation and application of some typical remotely sensed precipitation products in hydrology, meteorology, and hazard monitoring and forecast. Finally, we summarize current achievement and discuss the prospects of global satellite precipitation products.

Spaceborne and Ground-Based Sensors and Precipitation Retrievals

Review of Precipitation Sensors

Satellite sensors and ground weather radars are two main sources of remotely sensed rainfall. Satellite sensors include multichannels, such as visible and infrared (VIS/IR), passive microwave, and active microwave. Infrared sensors are generally onboard GEO which can provide precipitation estimates with relatively high temporal and spatial resolutions. Infrared data from the Geostationary Operational

Environmental Satellites (GOES) E/W; the Meteosat 5,7,8; and the Multifunctional Transport Satellites (MTSAT) have been widely used in various satellite precipitation products. FY-2 is the first generation of meteorological satellites in China, six geostationary satellites from FY-2A to FY-2F. Currently, FY-2 satellites have provided large amounts of data of precipitation, land surface, and sea surface temperature (http://fy3.satellite.cma.gov.cn/portalsite/default.aspx). Microwave data can be applied for more accurate rainfall estimation due to its more direct linkage with precipitation. The Advanced Microwave Sounding Unit (AMSU) onboard NOAA 10–12 and Special Sensor Microwave Imager (SSM/I) onboard Defense Meteorological Satellite Program (DMSP) F-13/14/15/16 are all popular passive microwave data sources.

Satellite-borne sensors are of great importance in estimating precipitation over the vast majority of the Earth's surface which lacks adequate in situ observing systems. Precipitation radars, such as TRMM PR, CloudSat CPR, and GPM DPR, can estimate precipitation best from space, while the orbit width of the three radars is very small (from 1.4 km for CPR to ~250 km for PR/DPR). Weather radars can provide accurate rainfall estimate on the ground. Combination of ground radars and rain gauges can generate precipitation products of high quality. All those satellite sensors and ground radars will be introduced detailed below.

Infrared Sensors

The Earth's surface, clouds, and atmosphere absorb solar energy and emit part of it into the outer space. The infrared sensors can sense these energies, which are often carried by GEO satellites, providing IR imagery 24 h a day with a high resolution (~ 4 × 4 km). There is an international constellation of GEO satellites covering the globe (Table 1), among which the Geostationary Operational Environmental Satellite system (GOES) operated by the National Oceanic and Atmospheric Administration (NOAA) is the primary one.

In the field of meteorology, radiation information collected by the IR sensors always relates to brightness temperature (T_b) of land surface, water surface, and

Table 1 Some geostationary satellites and sensors

Satellite	Agency	Sensor	Channels	Resolution (km)
GOES E/W	National Oceanic and Atmospheric Administration (NOAA)	GOES I-M Imager	5	1–4
Meteosat	European Organisation for the Exploitation of Meteorological Satellites (EUMETSAT)	MVIRI and SEVIRI	3–12	1–4
MTSAT/ Himawari	Japan Meteorological Agency (JMA)	Imager	5	1–5

cloud top. Most of IR-based rainfall estimation methods try to establish relationship model between surface rainfall rates and cloud-top brightness temperatures (Arkin 1979; Kummerow et al. 1998). According to the method used in processing the T_b values for different sensors, IR-based rainfall retrieval algorithms are divided into three main types, including pixel-based, window-based, and patch-based. The pixel-based algorithm is one of the most basic methods in satellite rainfall retrieval, and GOES Precipitation Index (GPI) is the most well-known one of them (Arkin and Meisner 1987). To improve the accuracy, the initial result is accumulated over a longer time scale (usually weekly or monthly) (Bastiaanssen et al. 1998; Liang et al. 2001).

The autoestimator (AE) algorithm utilizes a power law function to fit the Rainfall-T_b relationship. Further, researchers developed hydroestimator (HE) algorithm which takes more feature variables into account, such as relative humidity and precipitation water (Scofield and Kuligowski 2003). Besides the IR4 and IR5 channels, all other three channels of GOES Imager are used to modify the identification of raining clouds (Ba and Gruber 2001). Then, the rainfall rate of each raining cloud is assigned with the reference of its T_b. The cloud window-based algorithm is an extension of the pixel-based one. Hsu et al. (1997) developed the Precipitation Estimation from Remotely Sensed Information Using Artificial Neural Networks (PERSIANN) system, which relates pixel rainfall rate to a range of the neighborhood pixel coverage like a window (Hsu et al. 1997). The cloud window-based algorithm can involve in cloud local texture information based on T_b, making the retrieval more reasonable than the former two methods.

Cloud-patch-based algorithms extract feature information which may be related to rainfall rate from the entire cloud coverage. Various cloud segmentation approaches accompanied by pixel rainfall rate assignment tricks were developed. The Griffith-Woodley Technique (Griffith et al. 1978) assumes a specific T_b threshold under 253 K to separate cloud from IR T_b imagery. The Convective-Stratiform Technique (Adler and Negri 1988) firstly screens convective patches according to the local minimum value of T_b and assigns different rainfall amounts to convective clouds and stratiform clouds separately. Pixel rainfall rates are proportionally distributed according to the T_b inside cloud patches. Xu et al. (1999) used SSM/I microwave rainfall estimation to separate rain and no-rain pixels in a cloud patch, which made T_b thresholds variable in different situations (Xu et al. 1999). Hong et al. (2005) developed an automated neural network model named self-organizing nonlinear output (SONO) for patch-based rainfall estimation on the basis of PERSIANN system (Hong et al. 2005). The SONO model establishes various nonlinear T_b-Rainfall relations by classifying varied cloud patch into different clusters based on their extracted features which can be divided into three categories, i.e., coldness, geometry, and texture. The first category is directly associated with cloud brightness temperature (i.e., minimum and mean temperature of a cloud patch); the second one is derived from the geometric properties of cloud patches (i.e., cloud-path size and shape index); and the third category is the texture variation of cloud brightness temperature (i.e., standard deviation, mean value of local standard deviation, standard deviation of local standard deviation, and gradient).

Feature extraction is another important part of cloud-patch-based approaches. It's theoretically ideal to include as many features associated with land surface rainfall as possible. In PERSIANN-CCS system (Hong et al. 2004), nine key feature indices including the eight indices in Hong et al. (2005) which have been introduced above and gray image texture were extracted from cloud patches.

Microwave Sensors

Microwave sensors carried by LEO satellites have evolved steadily from the early Electronically Scanning Microwave Radiometer in the 1970s to the current SSM/I on DMSP satellites, the AMSU on the NOAA satellite series, the TRMM TMI, the Aqua Advanced Microwave Scanning Radiometer-Earth Observing System (AMSR-E) sensors, and the Global Precipitation Measurement (GPM) Microwave Imager (GMI). However, due to low temporal sampling resolution of passive microwave (PMW) data, significant coverage gaps exist even merging all of the available PMW datasets within every 3-h time window.

Rainfall from microwave sensors is estimated based on the principle that rainfall at the surface is related to microwave emission from raindrops at low-frequency channels and microwave scattering from ice at high-frequency channels (Kummerow et al. 1998). The satellite MW-based rainfall estimation algorithms can be roughly categorized into three classes: (1) the "emission"-type algorithms (Wilheit et al. 1991), which detect the increased radiances caused by rain over radiometrically cold oceans using low-frequency channels; (2) the "scattering" algorithms (Ferraro and Marks 1995), which correlate rainfall to radiance depressions caused by ice scattering present in many precipitating clouds; and (3) the "multichannel inversion"-type algorithms (Kummerow et al. 2001), which aim at inverting the entire radiance vector simultaneously.

The TMI as well as the AMSR-E uses the algorithms developed by Wilheit et al. (1991) and Kummerow et al. (2001), while the SSM/I uses the algorithms developed by Wilheit et al. (1991) and Ferraro and Marks (1995) in the GPCP over ocean and land, respectively. Precipitation estimation derived from the Advanced Microwave Sounding Unit-B (AMSU-B) at the National Environmental Satellite Data and Information Service (NESDIS) is supported by the algorithm developed by Weng et al. (2003). Each algorithm appears to have strengths and weaknesses related to specific applications, because they are optimized for the corresponding satellite sensor.

NASA GPM Integrated Multi-satellite Retrievals for GPM (IMERG), an advancement of TRMM TMPA, is an up-to-date product of global precipitation estimation. The algorithm used in GPM is transparent, parametric, and unified which ensures uniform rainfall products across all MW sensors from all satellite platforms. Huffman et al. (2015) suggests that the algorithm used in IMERG performs careful intercalibration of microwave estimates and provides finer time and space scales. Also, the robust algorithm including a generalized parametric framework which avoids the impasse of cross-evaluation of previous MW algorithms can attribute the differences between sensors to physical differences between observed scenes rather than artifacts of the algorithm.

Ground-Based Weather Radars

In order to address the growing interest in and demand for ground-based weather radars, this section serves as a guidance toward the understanding of this advanced instrument and relevant algorithms that constantly provides various kinds of meteorological data. The development of weather radars originated from World War II when radars were invented mainly for the battlefield (Buderi 1996; Brown 1999; Geiger 2008). With the advent of weather radars, our ability to detect high-resolution precipitation temporally and spatially has encountered unprecedented improvement, thus facilitating such application as flash flood forecasting and precipitation estimation (Doswell et al. 1996; Davis 2001; Krajewski and Smith 2002; Delrieu et al. 2005; Smith et al. 2007). For instance, with the radar systems available, not only regional-scale studies but also global-scale researches can be carried out. Recent decades have witnessed the invention of ground-based weather radars, enabling us to perform research and operations much more easily with radars.

Weather radars typically consist of the basic components: a klystron transmitter, a waveguide, an antenna, the pedestal, a feedhorn, a radome, and a receiver (Rinehart 1991; Doviak 1993). Weather Surveillance Radar-1988 Doppler (WSR-88D) that constitutes the NEXRAD network in operation across the United States is a widely used ground-based weather radar (Klazura and Imy 1993). The NEXRAD system is a network of 160 high-resolution Doppler weather radars operated by the National Weather Service, an agency of the National Oceanic and Atmospheric Administration (NOAA) within the US Department of Commerce. NEXRAD is capable of detecting precipitation and atmospheric movement or wind. When processed, the data returning can be displayed in a mosaic map which showcases patterns of precipitation and its movement. The greatest benefit of weather radars for hydrology lies in its potential to estimate rainfall rates at relatively high spatiotemporal resolution (i.e., 1 km/5 min), in real time, within a radius of approximately 250 km of the radar. Weather radar has enabled the transformation from a system of manual reporting and reacting to weather to one of the automated observations and anticipating weather impacts.

Steps for computing quantitative precipitation estimation (QPE) using conventional, single-polarization radar usually include the following. The first is radar calibration. The calibration of radar has a major influence on the accuracy of rainfall rates. A miscalibration of only 1 dB can result in bias in rainfall rates of 15%. Several methods for calibrating radar are provided in Atlas (2002). The second is quality control. Now that the Z data (radar reflectivity factor) have been bias-corrected for radar miscalibration, which requires large samples of comparisons over hours or even days of precipitation, every single bin of radar data must be carefully scrutinized to remove deleterious effects from non-meteorological scatters on the ground, biota in the atmosphere, planes, chaff, etc. The third is precipitation rate estimation. Calibrated reflectivity values illustrating the size, shape, state, and concentration of the hydrometeors within the radar sampling

volume are used subsequently to compute precipitation rate. In regions with complex terrain, bins are selected at multiple elevation angles to construct the hybrid scan for QPE. Reflectivity from the hybrid scan has made it possible to compute two-dimensional fields of precipitation rate in spherical coordinates (range, azimuth). The general form of reflectivity-to-rainfall relationships, or *Z-R* equations, is a power law as

$$Z = aR^b$$

where a is the prefactor and b is the exponent. The two most common *Z-R* relations are the NEXRAD default for convection ($a = 300$, $b = 1.4$) and the Marshall-Palmer relation ($a = 200$, $b = 1.6$) generally applied to stratiform rain (Marshall and Palmer 1948).

Global Multi-satellite Precipitation Products

Overview

A single sensor or single satellite can hardly provide global precipitation products with satisfying quality. Therefore, researchers have increasingly moved toward combining data from GEO VIS/IR and LEO MW sensors (Huffman et al. 2015; Wanders et al. 2015; Ashouri et al. 2015). A lot of such multi-satellite precipitation products have been developed and released to the public which are characterized by free access, quasi-global coverage, fine spatiotemporal resolutions, and continuous self-renewal, which, in turn, promote their development and applications (Tang et al. 2016b). The most commonly used satellite global rain products are summarized in Table 2. Most products provide both near-real-time and post-real-time datasets to satisfy different timeliness and quality requirement in climatology, meteorology,

Table 2 Summary of global satellite rainfall products

Product name	Agency/country	Spatial resolution	Temporal resolution	Period
GPCP	NASA/USA	2.5°	Monthly	1979–present
CMAP	NOAA/UAS	2.5°	5-day	1979–present
TMPA	NASA GSFC/USA	0.25°	3-hourly	1998–present
CMORPH	NOAA CPC/USA	0.25°/8 km	3-hourly/30-min	1998–present
PERSIANN	University of Arizona/USA	0.25°	3-hourly	2000–present
PERSIANN-CCS	University of California Irvine/USA	4 km	30-min	2006–present
PERSIANN-CDR	NOAA/USA	0.25°	Daily	1983–present
GSMaP	JAXA/Japan	0.1°	30-min	2014–present
IMERG	NASA/USA	0.1°	30-min	2014–present

hydrology, hazard forecast, etc. Compared with the information listed in Hong et al. (2012), the resolutions, periods, and accuracy of those products have been increased significantly in just a few years indicating the rapid advance of satellite remotely sensed precipitation. For example, the most recent IMERG products of the GPM mission are built on previous algorithms from PERSIANN-CCS, TMPA, and CMORPH which can provide three products at 30-min and 0.1° resolution between 60°N-S. Here we briefly introduce the algorithms and products of the three typical mainstream satellite precipitation products of PERSIANN-CCS, TMPA, and IMERG due to their widespread applications.

PERSIANN-CCS Algorithm

Through extracting local and regional cloud features from infrared (10.7 μm) geostationary satellite imagery, with microwave and ground radar rainfall data blending or training, the PERSIANN-CCS algorithm can provide fine-scale (4 km and 30-min) rainfall distribution. As shown in Fig. 1, the PERSIANN-CCS algorithm processes satellite cloud images into pixel rain rates by following four steps:

1. Segmentation of Satellite Infrared Cloud Images
   The incremental temperature threshold (ITT) is proposed to effectively segment cloud images which contain several convective cells into a large number of separated cloud patches by gradually increasing threshold temperatures. The ITT algorithm contains two main steps. First, the algorithm locates the local minimum temperature and initializes seeds. Second, the threshold temperature is set higher, and seeded regions are expanded from the seeded points until the border of other seeded regions or cloud-free regions is reached.
2. Extraction of Cloud-Patch Features
   A feature extraction scheme that retrieves both local pixel temperature textures and regional cloud-patch features instead of only local pixel features as in PERSIANN. Coldness, geometry, and texture are used to discriminate cloud types. Specifically, the coldness features of cloud patch include the minimum and mean temperature of a cloud patch; the geometric features include cloud-patch area and cloud-path shape index; and the texture features include standard deviation of cloud-patch temperature, mean value of local standard deviation of cloud temperature, standard deviation of local standard deviation of cloud, gradient of cloud-top brightness temperature, and gray image texture.
3. Classification of Cloud Patches
   The clouds are classified into different groups based on the cloud-patch features extracted from different temperature levels by a clustering algorithm, the self-organizing feature map (SOFM) (Hsu et al. 1997). SOFM projects the high-dimensional classification space of many input variables into various clusters arranged in a two-dimensional coordinate. Two main steps are involved. First, the distance between patch features and SOFM cluster center is calculated. Second,

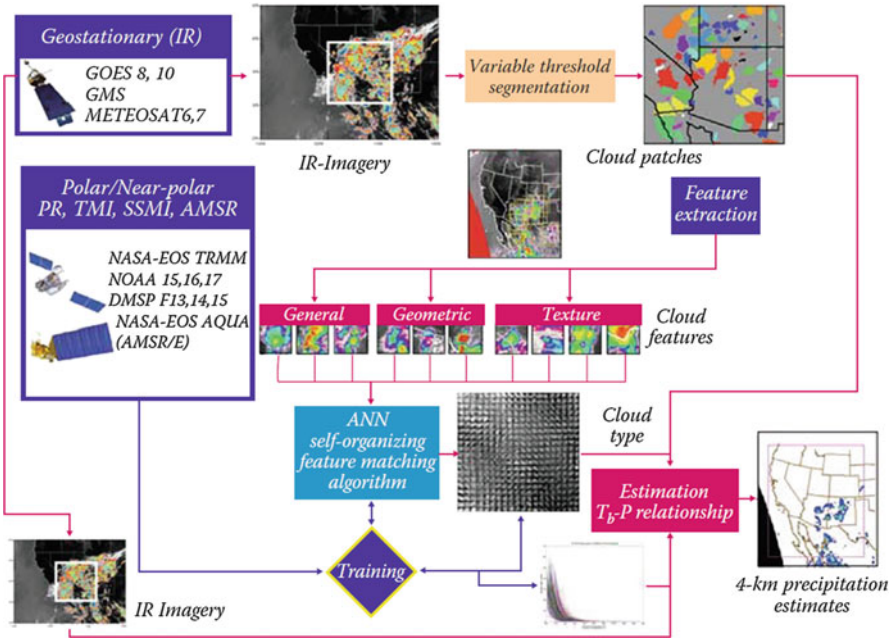

Fig. 1 Satellite cloud image segmentation, feature extraction, classification, multisensor blending, and rainfall estimation of the PERSIANN-CCS algorithm. (From Hong et al. (2012))

the best matching SOFM cluster center from the minimum distance between the input vector and the SORM connection weights is found.

4. Estimation of Patch and Pixel Rainfall
   Instead of calibrating only one T_b-R function for all clouds in PERSIANN, the PERSIANN-CCS searches a nonlinear T_b-R relationship for the full spectrum of cloud-rainfall conditions. Therefore, PERSIANN-CCS overcomes the limitation of a single statistical T_b-R function and can generate various rain rates at a given brightness temperature and variable rain/no-rain IR thresholds for different cloud types. In each classified cloud-patch group, the probability matching method is used to redistribute the T_b-R pixel pairs so that the proportion of the R distribution above a given rain rate is equal to the proportion of the T_b distribution below the associated T_b threshold value (Atlas et al. 1990). Then a nonlinear exponential function is fitted to the redistributed pixels, whose parameters are calibrated by numerous GOES infrared images and their collocated gauge-corrected radar rainfall.

The PERSIANN-CCS algorithm provides pixel rainfall distribution as well as cloud-rainfall system analysis basing on real-time GOES cloud images (Hong et al. 2004). Afterward, an automated neural network for cloud-patch-based rainfall

estimation, entitled SONO (Hong et al. 2005), was developed to adjust the T_b-R mapping function by using passive microwave precipitation estimates from low Earth orbiting satellite platforms, such as TRMM and Defense Meteorological Satellite Program. Evaluated at various temporal and spatial scales, PERSIANN-CCS shows good performance of estimation accuracy both in rain intensity and in the detection of rain/no-rain pixels (Hong et al. 2004, 2005, 2007). Real-time data from the current version of PERSIANN-CCS are available online both at regional and global scales (http://chrsdata.eng.uci.edu/).

TRMM-Based Multi-satellite Precipitation Analysis Algorithm

TMPA provides a calibration-based sequential scheme for combining precipitation estimates from multiple satellites, as well as gauge analyses where feasible, at $0.25° \times 0.25°$ and 3-hourly resolutions (Huffman et al. 2007). The TMPA provides a real-time product (3B42RT) and a gauge-adjusted post-real-time research product (3B42V7). The TMPA estimates are produced in four stages: (1) the MW precipitation estimates are calibrated and combined; (2) the IR precipitation estimates are created using the calibrated MW precipitation; (3) the MW and IR estimates are combined; and (4) the rain gauge data are incorporated.

Sources of passive microwave satellite precipitation estimates include TRMM TMI, SSM/I, Special Sensor Microwave Imager/Sounder (SSMIS) (3B42V7 only), AMSR-E, AMSU-B, and Microwave Humidity Sounder (MHS). The real-time product, 3B42RT, uses TMI estimates as the initial RT calibrator to calibrate precipitation estimates derived from available LEO MW radiometers and then merges all of the estimates at 3-h intervals. Gaps in the analyses are filled with GEO IR data regionally calibrated to the merged MW product. The post-real-time product, 3B42V7, adjusts the monthly accumulations of the 3-hourly fields from 3B42RT based on a monthly gauge analysis, including the new Global Precipitation Climatology Centre (GPCC) "full" gauge analysis whenever available and the GPCC "monitoring" gauge analysis since 2010. However, the previous monitoring product encompasses periods up to April 2005, and the Climate Assessment and Monitoring System (CAMS) analysis is used thereafter (Huffman et al. 2010). The final step of creating the research product is to introduce monthly rain gauge data. The monthly ratio of the satellite-only and satellite-gauge combination is used to rescale the individual 3-hourly estimates.

The TMPA intended to provide the "best" estimate of quasi-global precipitation. The most successful use of the TMPA data is that the analysis takes advantage of the fine-scale data to create time/space averages appropriate to the user's application. However, TMPA has some aspects that need to be improved which include improved error estimation and extension to higher latitudes (Li et al. 2009; Yong et al. 2013, 2014; Tang et al. 2016a, 2016b). After about 17 years of productive data gathering, the instruments on TRMM were turned off on April 8, 2015.

Integrated Multi-satellite Retrievals for GPM

The GPM mission has an international constellation of satellites, including one Core Observatory satellite and approximately ten partner satellites. The GPM Core Observatory was deployed on February 28, 2014, by a joint effort of NASA and the Japan Aerospace Exploration Agency (JAXA), marking a transition from the TRMM era to the GPM era. The GPM Core Observatory carries the DPR (the Ku-band at 13.6 GHz and Ka-band at 35.5 GHz) and GMI (frequencies range between 10 and 183 GHz). GPM extends the sensor package compared to TRMM instruments with the single-frequency PR (the Ku-band at 13.8 GHz) and TMI (frequencies range between 10 and 85.5 GHz). IMERG is a unified US algorithm, which is intended to intercalibrate, merge, and interpolate all microwave estimates of the GPM constellation, IR estimates, gauge observations, and other data from potential sensors at $0.1^\circ \times 0.1^\circ$ and half-hour temporal resolutions (Huffman et al. 2015). IMERG provides three kinds of products, including the near-real-time "Early" and "Late" run products, and the post-real-time "Final" run product. IMERG combines intermittent precipitation estimates from all constellation microwave sensors, IR-based observations from geosynchronous satellites, and monthly gauge precipitation data (Hou et al. 2014). IMERG employs the 2014 version of the Goddard Profiling Algorithm (GPROF2014) to compute precipitation estimates from all passive microwave (PMW) sensors onboard GPM satellites, which is an improvement compared with TMPA (GPROF2010) (Huffman et al. 2015). The IMERG "Final" run combines the GPCC Monitoring Product (currently Version 4) in the product, whose data source is limited to the Global Telecommunications System (GTS) with only about 7000 stations over the globe. The Full Data Reanalysis (currently Version 6) involves much more stations than the Monitoring Product but only covers the period 1901–2010. It is anticipated that the IMERG datasets would be reprocessed using the Full Data Reanalysis when it is updated to a longer period (Huffman et al. 2015). The IMERG data can be downloaded from the PMM website (http://pmm.nasa.gov/data-access/downloads/gpm). The IMERG product has been proved to be better than the previous TMPA products by some latest studies which will be introduced in detail in following sections.

Validation and Applications of Remote Sensing Precipitation

Regional and Global Assessment

The performance of Day-1 Integrated Multi-satellitE Retrievals for GPM IMERG and its predecessor, TRMM 3B42V7, was cross-evaluated using data from the best-available hourly gauge network over the Tibetan Plateau (TP) (Ma et al. 2016). IMERG Final run was used. Analyses of 3-hourly rainfall estimates in the warm season of 2014 reveal that IMERG shows appreciably better correlations and lower errors than 3B42V7, though with very similar spatial patterns for all assessment indicators. IMERG also appears to detect light rainfall better than 3B42V7.

However, IMERG shows the slightly lower probability of detection (POD) than 3B42V7 for elevations above 4200 m. Both IMERG and 3B42V7 successfully capture the northward dynamic life cycle of the Indian monsoon reasonably well over the TP. In particular, the relatively light rain from early and end Indian monsoon moisture surge events often fails to be captured by the sparsely distributed gauges. In spite of limited snowfall field observations, IMERG shows the potential of detecting solid precipitation, which cannot be retrieved from the 3B42V7 products (Fig. 2).

In addition, we also compare IMERG and 3B42V7 products over Mainland China using hourly rain data from around 2400 rain gauges (Tang et al. 2016b). The point gauge data are interpolated to areal precipitation field using the inverse distance weight (IDW) method. Both products agree well with the gauge data over East and South Mainland China. However, the correlation coefficient (CC) was a little lower over North China and even under 0.2 over West China. Several factors could contribute to relatively low CC of IMERG and 3B42V7 products over such areas: (1) the topography and climate over West China are complex, posing a great challenge for accurate satellite precipitation estimation; (2) the IMERG Final run was corrected using GPCC, whereas few gauges are used in the production of GPCC monthly gauge analysis in the TP, and thus the quality of IMERG products is potentially degraded; and (3) the interpolated precipitation could deviate far from the real values due to the sparse gauge networks, which would reduce reliability of metrics calculated against such ground reference. Figure 3 shows spatial distributions of CC, bias ratio (BIAS), and critical success index (CSI) computed from IMERG and 3B42V7 products against IDW interpolated precipitation at 3-hourly and $0.1^\circ \times 0.1^\circ$ resolutions over Mainland China. The distribution of CC seemed better for 3B42V7 than IMERG at the 3-hourly resolution (Fig. 3a–b). But at the daily resolution, IMERG performs better than 3B42V7 in North China.

The Coupled Routing and Excess Storage (CREST) model (Wang et al. 2011) is developed by the University of Oklahoma (http://hydro.ou.edu) and the NASA SERVIR Project Team (www.servir.net). The CREST model has been implemented successfully in a variety of multi-scale meteorological and hydrological studies (Tang et al. 2016c; Kan et al. 2017; Li et al. 2017). The CREST V2.1 (Shen et al. 2016) is used to evaluate the quality of IMERG as well as its hydrological continuity compared with TRMM era products (TMPA 3B42V7 and 3B42RT) in the Ganjiang River basin, which is the seventh largest sub-catchment of the Yangtze River. The China Gauge-based Daily Precipitation Analysis (CGDPA) product is used as the ground truth (Shen and Xiong 2016).

In the validation period (May 1, 2014–September 30, 2014), the CREST model was forced by CGDPA, 3B42V7, 3B42RT, and IMERG precipitation data based on parameter calibrated by CGDPA from 2003 to 2009. CGDPA has the best skill scores in terms of streamflow simulation as expected, closely followed by IMERG (IMERG/CGDPA: NSCE = 0.77/0.86, CC = 0.91/0.94, BIAS = −14.09/−8.76%, and RMSE = 1080.87/822.73m^3/s). The hydrograph of IMERG is remarkably similar to that of CGDPA (Fig. 4a and b). Compared with 3B42V7 and 3B42RT, IMERG performed the best and matched well with the observed streamflow,

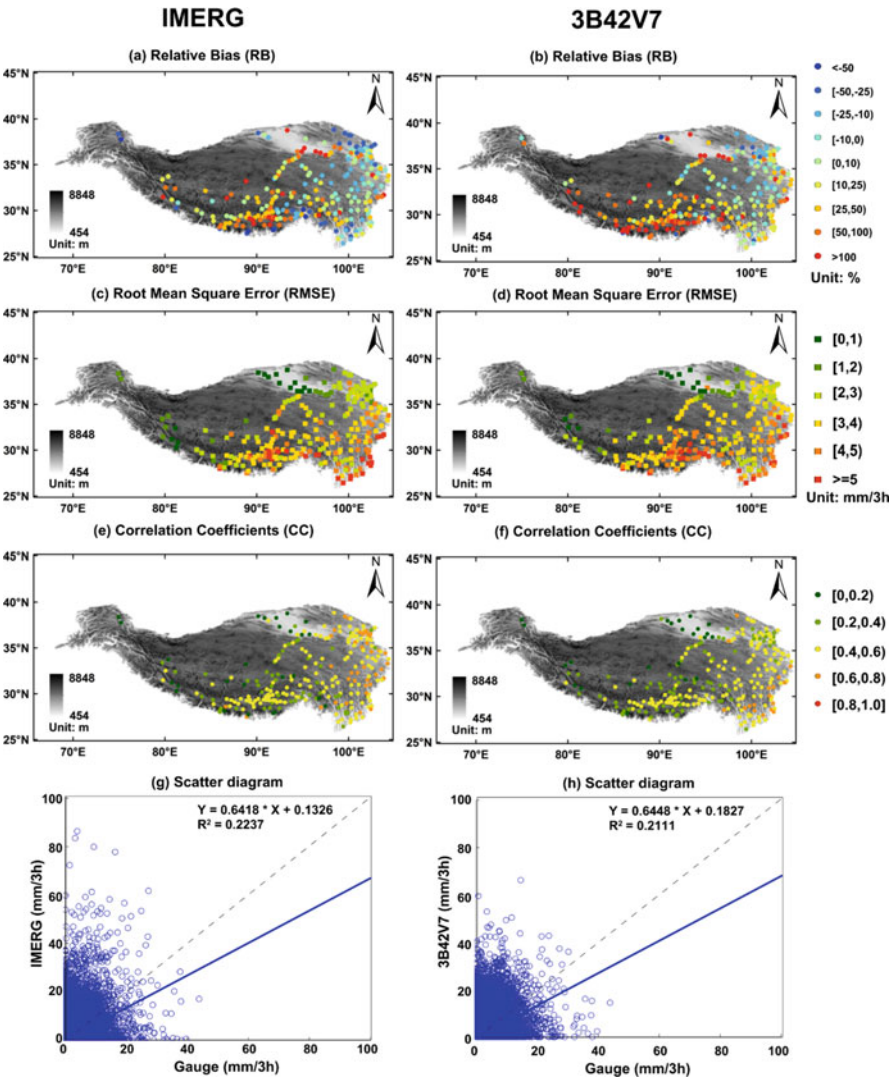

Fig. 2 Maps of (**a**–**b**) relative bias (RB), (**c**–**d**) root mean square error (RMSE), (**e**–**f**) correlation coefficients (CC), and (**g**–**h**) scatter diagram between satellite- and gauge-based 3-hourly rainfall estimates in the warm season (April–September) of 2014 over the TP. Notes: the left panel, i.e., (**a**, **c**, **e**, **g**), stands for IMERG rainfall estimates, and the right panel, i.e., (**b**, **d**, **f**, **h**) stands for 3B42V7 products. (From Ma et al. 2016)

especially for the second flow peak compared with 3B42V7 and 3B42RT (Fig. 4b–d). The 3B42RT product came at the bottom as its NSCE declined to 0.46 and RMSE increased to 1637.53 m^3/s.

The accuracy of satellite precipitation products varies with regions. Therefore, although regional validation studies can help reveal the error characteristics of some

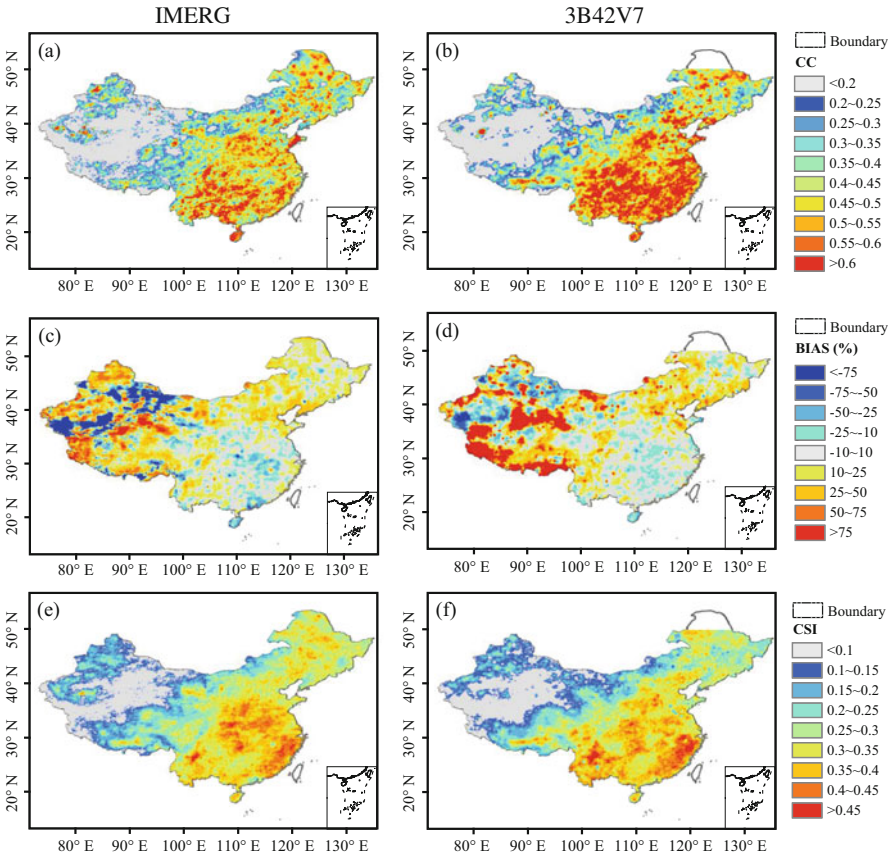

Fig. 3 Spatial distributions of assessment metrics for IMERG (the left panel) and 3B42V7 (the right panel) precipitation at 3-hourly and 0.1° × 0.1° resolution over Mainland China: (**a**–**b**) CC, (**c**–**d**) BIAS, and (**e**–**f**) CSI. (From Tang et al. 2016a)

satellite products, global evaluation and comparison are necessary. Beck et al. (2017) evaluated the performance of 23 precipitation products in the global scale using 76,086 gauges worldwide. A conceptual hydrological model HBV is employed to evaluate the ten gauge-corrected datasets in 9053 small- to medium-sized basins to avoid the independence problem caused by overlapped gauges. However, it is hard for researchers to obtain worldwide ground observations. Massari et al. (2017) uses the triple collocation (TC) method to characterize uncertainties of satellite precipitation products in the globe. The TC method requires the input of three independent datasets and can output the error statistics of input datasets. In addition, some studies try to evaluate satellite precipitation products by using data from spaceborne radars as the benchmark due to their high accuracy than passive microwave and infrared sensors. For example, Behrangi et al. (2014) evaluated the capability of spaceborne sensors in detecting light precipitation and snowfall using CloudSat Cloud Profiling

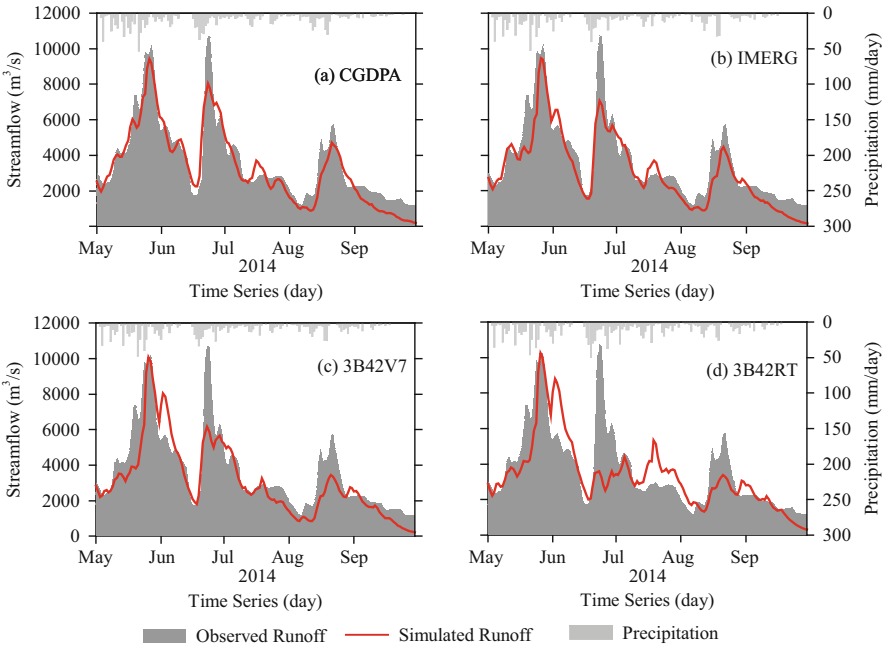

Fig. 4 Comparison of CREST simulated streamflow with gauge-calibrated parameters and observed streamflow validation period 2 (May 1, 2014–September 30, 2014). (**a**) Daily data from CGDPA; (**b**) daily data from IMERG; (**c**) daily data from 3B42V7; and (**d**) daily data from 3B42RT. (From Tang et al. 2016c)

Radar (CPR). Tang et al. (2017) intercompared the rainfall and snowfall performance of the three existing spaceborne precipitation radars, i.e., TRMM PR, GPM DPR, and CloudSat CPR.

Application in Flood Detection and Prediction

Satellite precipitation products can be applied in hydrologic studies to predict flood events (Khan et al. 2011). Wang et al. (2011) established a real-time Global Hydrological Prediction System (GHPS) with the CREST model to investigate the detectability and predictability of flooding (Fig. 5). GHPS is forced by the NASA Tropical Rainfall Measuring Mission (TRMM) Multi-satellite Precipitation Analysis at near-real-time and by the deterministic and ensemble precipitation forecast products from NOAA Global Forecast System (GFS) at several lead times (Zhang et al. 2015). The CREST model is currently running within the near-real-time global hydrological simulation and flood monitoring demonstration system (http://eos.ou.edu) at the University of Oklahoma. Presently, it is driven by the TRMM 3B42RT. Another global flood system is Global Flood Monitoring System (GFMS; http://flood.umd.edu/) (Wu et al. 2014) which is supported by TMPA and GPM products.

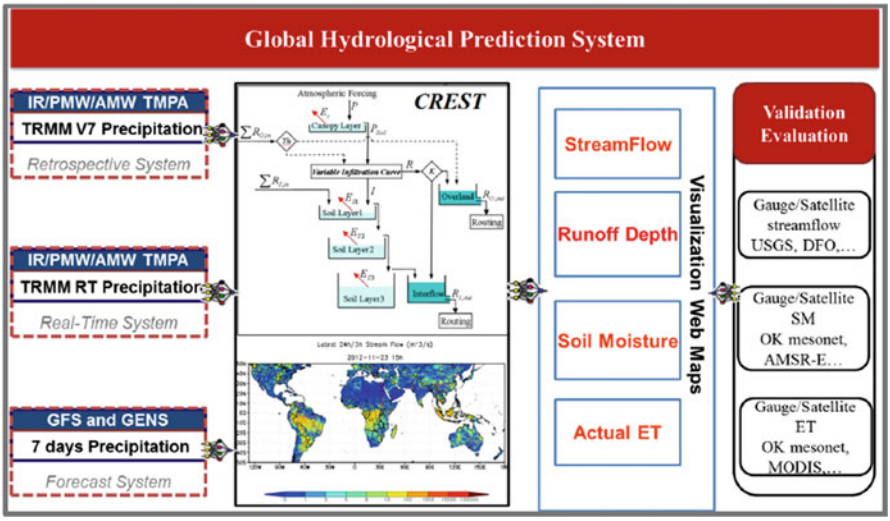

Fig. 5 Structure of the Global Hydrological Prediction System. (From Zhang et al. 2015)

GFMS has played an important role in flood monitoring and can be utilized for decision support (Kirschbaum et al. 2017).

Floods usually lead to huge casualties and damages to urban areas due to its high population density and intensively developed infrastructure. Moreover, the impervious surface in urban areas would also increase the runoff rate. Thus, it is an emergency to predict urban to reduce their impacts. For example, the flood event on July 21, 2012, in Beijing, the Capital City of China, is detected and predicted by the GHPS. The "7·21" Beijing storm lasted for around 16 h, and the rain rate reached as high as 215 mm/day in the urban areas, resulting in 79 fatalities and around 1.6 billion dollars of damages. We used rain gauge observations, TRMM RT, TRMM V7, and both GFS deterministic and ensemble precipitation forecasts at different initializations (with different lead times, as in Table 3) to simulate the hydrological predictions of surface runoff in urban areas and streamflow in the watersheds in Beijing. Before the simulation, soil states in the global CREST model are initialized by running the model using TRMM RT rainfall forcing from July 1, 2012, until the initial time of each experiment. Results indicate that the disastrous "7·21" storm was detectable by TRMM satellite precipitation estimates and predictable by deterministic GFS rainfall forecasts at least 4 days in advance.

In flash flood warning and forecasting, remotely sensed rainfall can provide useful information to determine when and how to make alerts and take evacuation actions. Based on the widely used Flash Flood Guidance (FFG) system (Georgakakos 1987), we developed a Cascading Flash Flood Guidance (CFFG) system, progressively from the Flash Flood Potential Index (FFPI), the Flash Flood Hazard Index (FFHI), and the Flash Flood Risk Index (FFRI) (Zeng et al. 2006). Together with the land cover, vegetation cover, SRTM slope, and soil

Table 3 Summary of characteristics of the precipitation products used in the detecting and predicting of the "7·21" Beijing event[a]

Rainfall products	Spatial resolution	Time interval	Lead time	Reference
Rain Gauge Observation	Interpolated onto 0.25°	Hourly; then accumulated to 3-hourly	N/A	Huffman et al. 2007
TRMM RT	0.25°	3-hourly	N/A	
TRMM RP	0.25°	3-hourly	N/A	
Deterministic GFS Precipitation	0.25°	3-hourly	180 h	Wang 2010; Wang et al. 2013
Ensemble GFS Precipitation	0.25°	3-hourly	168 h	

[a]From Zhang et al. (2015)

property data for the FFPI calculation, average daily amount in flood seasons and maximum 6 h and maximum 24 h amount from TRMM V7 are used as rainfall effect indicators to determine the relative hazard potential of flash flood, which is represented by the value of FFHI (ranging from 1 to 10, 1 means lowest potential and 10 the highest). The weights between indicators are determined by an integrated approach of the analytic hierarchy process and the information entropy theory. Further inclusion of GDP, population, and flood prevention measures as vulnerability factors for the FFRI enables the prediction of the flash flood risk. Until now, the CFFG system has been implemented in a fine resolution (1 km) in Yunnan Province, and the characteristics of China's flash floods are also mapped in a cascading manner.

Conclusive Remarks and Outlooks

The rapid development of remote sensing techniques has made precipitation estimation more accurate and cover broader regions compared with traditional rain gauges around the world. Satellite-based precipitation products supported by VIS/IR and passive/active MW sensors promote our knowledge of global water and energy cycle. Currently, the newest GPM based on the heritage of precedent multi-satellite algorithms such as TMPA, CMORPH, and PERSIANN-CCS has released its Level-1 to Level-3 data to the public for more than 2 years. The Level-4 products combining with models are also anticipated to be developed and released in the future, and the spatial coverage could be extended to near 90°N/S compared with 60°N/S of current products. However, satellite precipitation products still have some way to go in further improving its quality in high mountains (such as the TP), high latitude regions, and arid regions.

Active microwave sensors can estimate precipitation with comparable quality with ground gauges and radars. However, after the TRMM PR was decommissioned, only two precipitation radars operate in space. The future development of

spaceborne radars has two complementary directions, multi-frequency radar instruments on single platform and constellation of many small to cube radar satellites, for improved global precipitation estimation. The employment of more spaceborne radar data is the future trend of achieving accurate enough estimation of global rainfall and snowfall only based on satellites. In addition, future radar design should consider including more bands on a single platform, such as Ka-, Ku-, and W-bands. Jet Propulsion Laboratory (JPL) has developed an architecture with a low-cost simplified spaceborne radar system, namely, RainCube (Peral et al. 2015). The inexpensive CubeSats can compose a constellation with a number of satellites monitoring the earth frequently. Together with the advanced but expensive big spaceborne radars, estimation of global rainfall and snowfall can be greatly improved.

Acknowledgment This study was financially supported by the National Natural Science Foundation of China (Grant No. 71461010701), National Key Research and Development Program of China (2016YFE0102400), and National Natural Science Foundation of China (Grant No. 91437214).

References

R.F. Adler, A.J. Negri, A satellite infrared technique to estimate tropical convective and stratiform rainfall. J. Appl. Meteorol. **27**, 30–51 (1988)

P.A. Arkin, The relationship between fractional coverage of high cloud and rainfall accumulations during GATE over the B-scale array. Mon. Weather Rev. **107**(10), 1382–1387 (1979)

P.A. Arkin, B.N. Meisner, The relationship between large-scale convective rainfall and cold cloud over the western hemisphere during 1982–84. Mon. Weather Rev. **115**, 51–74 (1987)

H. Ashouri, K.L. Hsu, S. Sorooshian, et al., PERSIANN-CDR: Daily precipitation climate data record from multisatellite observations for hydrological and climate studies. J. Bull. Am. Meteorol. Soc. **96**(1), 69–83 (2015)

D. Atlas, Radar calibration: Some simple approaches. Bull. Am. Meteorol. Soc. **83**(9), 1313 (2002)

D. Atlas, D. Rosenfeld, D.B. Wolff, Climatologically tuned reflectivity-rain rate relations and links to area-time integrals. J. Appl. Meteorol. **29**, 1120–1135 (1990)

M. Ba, A. Gruber, GOES multispectral rainfall algorithm (GMSRA). J. Appl. Meteorol. **40**, 1500–1514 (2001)

W.G.M. Bastiaanssen, H. Pelgrum, J. Wang, et al., A remote sensing surface energy balance algorithm for land (SEBAL): Part 2: Validation. J. Hydrol. **212**, 213–229 (1998)

H.E. Beck et al., Global-scale evaluation of 23 precipitation datasets using gauge observations and hydrological modeling. Hydrol. Earth Syst. Sci. Discuss., 1–23 (2017)

A. Behrangi et al., What does CloudSat reveal about global land precipitation detection by other spaceborne sensors? Water Resour. Res. **50**(6), 4893–4905 (2014)

A. Berne, G. Delrieu, J.D. Creutin, C. Obled, et al., Temporal and spatial resolution of rainfall measurements required for urban hydrology. J. Hydrol. **299**(3–4), 166–179 (2004)

L. Brown, A radar history of World War II. J. Am. Hist. Res. (1999)

R. Buderi, *The Invention that Changed the World: How a Small Group of Radar Pioneers Won the Second World War and Launched a Technological Revolution* (Simon and Schuster, New York, 1996)

R.S. Davis, Flash flood forecast and detection methods, in *Severe Convective Storms*, (American Meteorological Society, Boston, 2001), pp. 481–525

G. Delrieu, J. Nicol, E. Yates, et al., The catastrophic flash-flood event of 8–9 September 2002 in the Gard region, France: A first case study for the Cévennes–Vivarais Mediterranean Hydrometeorological Observatory. J. Hydrometeorol. **6**(1), 34–52 (2005)
C.A. Doswell, H.E. Brooks, R.A. Maddox, Flash flood forecasting: An ingredients-based methodology. J. Weather Forecast. **11**(4), 560–581 (1996)
R.J. Doviak, *Doppler Radar and Weather Observations* (Courier Corporation, Chelmsford, 1993)
L.H.Z.P.N. Fang, H.S.Z.X.G. Runsheng, X. Bao, China operational weather radar data processing system. J. Appl. Meteorlol. **6**, 014 (2002)
F. Farbry, A. Bellon, M.R. Duncan, G.L. Austin, et al., High resolution rainfall measurements by radar for very small basins: The sampling problem reexamined. J. Hydrol. **161**(1–4), 415–428 (1994)
R. Ferraro, G. Marks, The development of SSM/I rain-rate retrieval algorithms using ground-based radar measurements. J. Atmos. Ocean Technol. **12**(4), 755–770 (1995)
R.L. Geiger, *Research and Relevant Knowledge: American Research Universities Since World War II* (Transaction Publishers, New Brunswick, 2008)
K.P. Georgakakos, Real-time flash flood prediction. J. Geophys. Res. Atmos. **92**(D8), 9615–9629 (1987)
C.G. Griffith, W.L. Woodley, P.G. Grube, D.W. Martin, J. Stout, D.N. Sikdar, Rain estimation from geosynchronous satellite imagery-visible and infrared studies. Mon.Weather Rev. **106**, 1153–1171 (1978)
D. Harris, E. Foufoula-Georgiou, K. Droegemeier, et al., Multiscale statistical properties of a high-resolution precipitation forecast. J. Hydrometeorol. **2**(4), 406–418 (2001)
W.H. Heiss, D.L. McGrew, D. Sirmans, et al., NEXRAD: Next generation weather radar (WSR-88D). J. Microwave **33**(1), 79–89 (1990)
Y. Hong, K.L. Hsu, S. Sorooshian, et al., Precipitation estimation from remotely sensed imagery using an artificial neural network cloud classification system. J. Appl. Meteorol. **43**, 1834–1853 (2004)
Y. Hong, K. Hsu, S. Sorooshian, et al., Self-organizing nonlinear output (SONO): A neural network suitable for cloud patch–based rainfall estimation at small scales. Water Resour. Res. **41**, 477–490 (2005)
Y. Hong, D. Gochis, J. Cheng, et al., Evaluation of PERSIANN-CCS rainfall measurement using the NAME event rain gauge network. J. Hydrometeorol. **8**, 469–482 (2007)
Y. Hong, S. Chen, X. Xue, G. Hodges, Global precipitation estimation and applications, in *Multiscale Hydrologic Remote Sensing: Perspectives and Applications*, (CRC Press, Boca Raton, 2012), pp. 371–386
Y. Hong, Y. Zhang, S. Khan, *Hydrologic Remote Sensing: Capacity Building for Sustainability and Resilience* CRC Press, (2016)
A.Y. Hou, R.K. Kakar, S. Neeck, A.A. Azarbarzin, C.D. Kummerow, M. Kojima, . . . T. Iguchi, The global precipitation measurement mission. J. Am. Meteorol. Soc. **95**(5), 701–722 (2014)
K. Hsu, X. Gao, S. Sorooshian, H.V. Gupta, Precipitation estimation from remotely sensed information using artificial neural networks. J. Appl. Meteorol. **36**, 1176–1190 (1997)
G.J. Huffman, D.T. Bolvin, E.J. Nelkin, D.B. Wolff, R.F. Adler, G. Gu, . . . E.F. Stocker, The TRMM multisatellite precipitation analysis (TMPA): Quasi-global, multiyear, combined-sensor precipitation estimates at fine scales. J. Hydrometeorol. **8**, 38–55 (2007)
G.J. Huffman, R.F. Adler, D.T. Bolvin, E.J. Nelkin, The TRMM multi-satellite precipitation analysis (TMPA), in *Satellite Rainfall Applications for Surface Hydrology*, (Springer Netherlands, Dordrecht, 2010), pp. 3–22
G.J. Huffman, D.T. Bolvin, E.J. Nelkin, Integrated Multi-satellitE Retrievals for GPM (IMERG) Technical Documentation. NASA/GSFC Code 612, 47 pp. http://pmm.nasa.gov/sites/default/files/document_files/IMERG_doc.pdf (2015)
R.J. Joyce, J.E. Janowiak, P.A. Arkin, P. Xie, CMORPH: A method that produces global precipitation estimates from passive microwave and infrared data at high spatial and temporal resolution. J. Hydrometeorol. **5**(3), 487–503 (2004)

G. Kan, G. Tang, Y. Yang, Y. Hong, J. Li, L. Ding, et al., An improved coupled routing and excess storage (CREST) distributed hydrological model and its verification in Ganjiang River basin, China. Water **9**(11), 904 (2017)

I.S. Khan et al., Satellite remote sensing and hydrologic modeling for flood inundation mapping in Lake Victoria basin: Implications for hydrologic prediction in ungauged basins. IEEE Trans. Geosci. Remote Sens. **49**, 85–95 (2011)

C. Kidd, G. Huffman, Global precipitation measurement. Meteorol. Appl. **18**, 334–353 (2011)

D.B. Kirschbaum, G.J. Huffman, R.F. Adler, S. Braun, K. Garrett, E. Jones, et al., NASA's remotely sensed precipitation: A reservoir for applications users. Bull. Am. Meteorol. Soc. **98**(6), 1169–1184 (2017)

G.E. Klazura, D.A. Imy, A description of the initial set of analysis products available from the NEXRAD WSR-88D system. J. Am. Meteorol. Soc. **74**(7), 1293–1311 (1993)

W.F. Krajewski, J.A. Smith, Radar hydrology: Rainfall estimation. J. Adv. Water Resour. **25**(8–12), 1387–1394 (2002)

T. Kubota, S. Shige, H. Hashizume, K. Aonashi, N. Takahashi, S. Seto, ... K. Iwanami. Global precipitation map using satellite-borne microwave radiometers by the GSMaP project: Production and validation. IEEE T. Geosci. Remote. **45**(7), 2259–2275 (2007)

C. Kummerow, W. Barnes, T. Kozu, et al., The tropical rainfall measuring mission (TRMM) sensor package. J. Atmos. Ocean. Technol. **15**(3), 809–817 (1998)

C. Kummerow, Y. Hong, W. Olson, et al., The evolution of the Goddard Profiling Algorithm (GPROF) for rainfall estimation from passive microwave sensors. J. Appl. Meteorol. **40**(11), 1801–1820 (2001)

L. Li, Y. Hong, J. Wang, et al., Evaluation of the real-time TRMM-based multi-satellite precipitation analysis for an operational flood prediction system in Nzoia Basin, Lake Victoria, Africa. J. Nat. Hazards **50**(1), 109–123 (2009)

N. Li, G. Tang, P. Zhao, Y. Hong, Y. Gou, K. Yang, Statistical assessment and hydrological utility of the latest multi-satellite precipitation analysis IMERG in Ganjiang River basin. Atmos. Res. **183**, 212–223 (2017)

L. Liang, C. Liu, Y.Q. Xu, et al., Real-time texture synthesis by patch-based sampling. J. ACM Trans. Graphics (ToG) **20**(3), 127–150 (2001)

Y. Ma, G. Tang, D. Long, B. Yong, L. Zhong, W. Wan, Y. Hong, Similarity and error intercomparison of the GPM and its predecessor-TRMM multisatellite precipitation analysis using the best available hourly gauge network over the Tibetan plateau. Remote Sens. **8**(7), 569 (2016)

J.S. Marshall, W.M.K. Palmer, The distribution of raindrops with size. J. Meteor. **5**(4), 165–166 (1948)

C. Massari et al., An assessment of the performance of global rainfall estimates without ground-based observations. Hydrol. Earth Syst. Sci. **21**(9), 4347–4361 (2017)

J. Morin, D. Rosenfeld, E. Amitai, et al., Radar rain field evaluation and possible use of its high temporal and spatial resolution for hydrological purposes. J. Hydrol. **172**(1–4), 275–292 (1995)

E. Peral, S. Tanelli, Z. Haddad, et al., Raincube: A proposed constellation of precipitation profiling radars in CubeSat, in *C. Geoscience and Remote Sensing Symposium (IGARSS), 2015 I.E. International*, (IEEE, 2015), Milan, Italy, pp. 1261–1264

R.E. Rinehart, *Radar for Meteorologists* (University of North Dakota, Office of the President, 1991). Grand Forks, North Dakota

R.A. Scofield, R.J. Kuligowski, Status and outlook of operational satellite precipitation algorithms for extreme-precipitation events. Mon. Weather Rev. **18**, 1037–1051 (2003)

Y. Shen, A. Xiong, Validation and comparison of a new gauge-based precipitation analysis over mainland China. Int. J. Climatol. **36**(1), 252–265 (2016)

X. Shen, Y. Hong, K. Zhang, Z. Hao, Refining a distributed linear reservoir routing method to improve performance of the CREST model. J. Hydrol. Eng. **22**, 04016061 (2016)

A.I. Shiklomanov, R.B. Lammers, C.J. Vörösmarty, Widespread decline in hydrological monitoring threatens pan-arctic research. Eos, Trans. Am. Geophys. **83**(2), 13–17 (2002)

J. Simpson, R.F. Adler, G.R. North, A proposed tropical rainfall measuring mission (TRMM) satellite. J. Am. Meteorol. Soc. **69**(3), 278–295 (1988)
J.A. Smith, M.L. Baeck, K.L. Meierdiercks, et al., Radar rainfall estimation for flash flood forecasting in small urban watersheds. J. Adv. Water Resour. **30**(10), 2087–2097 (2007)
T.M. Smith, V. Lakshmanan, G.J. Stumpf, et al., Multi-radar multi-sensor (MRMS) severe weather and aviation products: Initial operating capabilities. J. Am. Meteorol. Soc. **97**(9), 1617–1630 (2016)
S. Sorooshian, K.L. Hsu, X. Gao, H.V. Gupta, B. Imam, D. Braithwaite, Evaluation of PERSIANN system satellite-based estimates of tropical rainfall. Bull. Am. Meteor. Soc. **81**(9), 2035–2046 (2000)
E. Stokstad, Scarcity of rain, stream gages threatens forecasts. Science **285**(5431), 1199–1200 (1999)
G. Tang, Y. Ma, D. Long, L. Zhong, Y. Hong, Evaluation of GPM Day-1 IMERG and TMPA Version-7 legacy products over mainland China at multiple spatiotemporal scales. J. Hydrol. **533**, 152–167 (2016a)
G. Tang, D. Long, Y. Hong, Systematic anomalies over inland water bodies of High Mountain Asia in TRMM precipitation estimates: No longer a problem for the GPM era? IEEE Geosci. Remote Sens. **13**, 1762 (2016b)
G. Tang, Z. Zeng, D. Long, X. Guo, B. Yong, W. Zhang, Y. Hong, Statistical and hydrological comparisons between TRMM and GPM Level-3 products over a Midlatitude Basin: Is Day-1 IMERG a good successor for TMPA 3B42V7? J. Hydrometeorol. **17**(1), 121–137 (2016c)
G. Tang et al., Similarities and differences between three coexisting spaceborne radars in global rainfall and snowfall estimation. Water Resour. Res. **53**(5), 3835–3853 (2017)
J. Vivekanandan, S.M. Ellis, R. Oye, et al., Cloud microphysics retrieval using S-band dual-polarization radar measurements. J. Am. Meteorol. Soc. **80**(3), 381–388 (1990)
N. Wanders, M. Pan, E.F. Wood, Correction of real-time satellite precipitation with multi-sensor satellite observations of land surface variables. J. Remote Sens. Environ. **160**, 206–221 (2015)
X. Wang, Incorporating ensemble covariance in the gridpoint statistical interpolation variational minimization: A mathematical framework. Mon. Weather Rev. **138**(7), 2990–2995 (2010)
J. Wang, Y. Hong, L. Li, et al., The coupled routing and excess storage (CREST) distributed hydrological model. Hydrol. Sci. J. **56**(1), 84–98 (2011)
X. Wang, D. Parrish, D. Kleist, et al., GSI 3DVar-based ensemble–variational hybrid data assimilation for NCEP global forecast system: Single-resolution experiment. Mon. Weather Rev. **141**(11), 4098–4117 (2013)
F. Weng, L. Zhao, R. Ferraro, et al., Advanced microwave sounding unit cloud and precipitation algorithms. Radio Sci. **38**(4), 8068 (2003)
T. Wilheit, A. Chang, L. Chiu, Retrieval of monthly rainfall indices from microwave radiometric measurements using probability distribution functions. J. Atmos. Ocean Technol. **8**(1), 118–136 (1991)
H. Wu, R.F. Adler, Y. Tian, G.J. Huffman, et al., Real-time global flood estimation using satellite-based precipitation and a coupled land surface and routing model. Water Resour. Res. **50**(3), 2693–2717 (2014)
L. Xu, X. Gao, S. Sorooshian, P.A. Arkin, A microwave infrared threshold technique to improve the GOES precipitation index. J. Appl. Meteorol. **38**, 569–579 (1999)
B. Yong, L. Ren, Y. Hong, et al., First evaluation of the climatological calibration algorithm in the real-time TMPA precipitation estimates over two basins at high and low latitudes. J. Water Resour. Res. **49**(5), 2461–2472 (2013)
B. Yong, B. Chen, J.J. Gourley, et al., Intercomparison of the Version-6 and Version-7 TMPA precipitation products over high and low latitudes basins with independent gauge networks: Is the newer version better in both real-time and post-real-time analysis for water resources and hydrologic extremes? J. Hydrol. **508**, 77–87 (2014)
Z. Zeng, G. Tang, D. Long, et al., A cascading flash flood guidance system: development and application in Yunnan Province, China. Natural Hazards, 84(3), 2071–2093
Y. Zhang, Y. Hong, X. Wang, et al., Hydrometeorological analysis and remote sensing of extremes: Was the July 2012 Beijing flood event detectable and predictable by global satellite observing and global weather modeling systems? J. Hydrol. **16**(1), 381–395 (2015)